Journal of Luminescence 207 (2019) 435–442

Contents lists available at ScienceDirect

Journal of Luminescence

journal homepage: www.elsevier.com/locate/jlumin

Fine structure in high resolution $4f^7$–$4f^6$5d excitation and emission spectra of X-ray induced Eu^{2+} centers in $LuPO_4$:Eu sintered ceramics

Justyna Zeler[a], Andries Meijerink[b], Dagmara Kulesza[a], Eugeniusz Zych[a,*]

[a] Faculty of Chemistry, University of Wroclaw, 14 F. Joliot-Curie Street, 50-383 Wroclaw, Poland
[b] Condensed Matter and Interfaces, Debye Institute for Nanomaterials Science, Utrecht University, Princetonplein 1, 3584 CC, Utrecht, the Netherlands

ARTICLE INFO

Keywords:
$LuPO_4$
Eu^{2+} luminescence
Zero-phonon line
$4f^6$5d excited state
High resolution spectroscopy

ABSTRACT

X-ray induced effects in $LuPO_4$:Eu^{3+} sintered thermoluminescent material were investigated by absorption and photoluminescence measurements between 20 and 300 K. Evidence for Eu^{3+}→Eu^{2+} conversion upon exposure to X-rays was obtained as narrow band blue Eu^{2+} photoluminescence was observed. The low temperature luminescence of Eu^{2+} ions in X-rayed $LuPO_4$:Eu ceramics showed a unique fine structure with a sharp zero-phonon line at 425.8 nm and well-resolved vibronic structure. Excitation spectra of the Eu^{2+} luminescence revealed a rich structure in which individual $4f^7$→ $4f^6(^7F_J)5d^1$ zero-phonon lines accompanied by vibronic transitions were identified. A detailed analysis allowed an accurate calculation of the Eu^{3+}-like 4 $f^6(^7F_J)$ core levels in the 4 $f^6$5d^1 excited configuration. The $4f^6$ core splitting is different from that of the ^7F_J states for Eu^{3+} in $LuPO_4$, providing evidence for the role of $4f^6$–5d interaction on the splitting of the $4f^6$ configuration. The unique luminescence of Eu^{2+} with a small Stokes shift and well-determined energies of $4f^6(^7F_J)5d^1$ excited states make $LuPO_4$:Eu a model system for testing theoretical models which are presently developed to calculate and predict the energy level structure and Stokes shift of $4f^n$–$4f^{n-1}5d^1$ transitions of lanthanides.

1. Introduction

Orthophosphates activated with lanthanide ions have been well-known for years as efficient luminescent materials and e.g. micro-crystalline $LaPO_4$:Ce,Tb is a widely applied lamp phosphor [1–6]. Yet, classic techniques of making large singly crystals could not be applied for these compositions as they melt incongruently and/or decompose upon liquefying. Only needle shaped crystals of several mm long have been reported. This restricts possible areas of their applications [7].

These problems encouraged us to fabricate rare earths doped $LuPO_4$ ceramic bodies by high-temperature sintering to remove porosity and achieve an effective density and transparency close to that of single crystals. Ceramics were obtained upon classic vacuum sintering and some properties of these sintered materials were published previously [8–10]. After irradiation with X-rays, the high-temperature processed $LuPO_4$:Eu sintered ceramics showed an efficient thermoluminescence (TL) with maximum intensity about 200 °C [8–11]. The 3D temperature and wavelength resolved thermoluminescence of X-rayed $LuPO_4$:0.1% Eu together with main part of its EPR spectrum is presented in Fig. 1 [10].

The TL emission shown in Fig. 1 is typical for Eu^{3+} luminescence in $LuPO_4$ and results from transitions from $^5D_0$ excited state to the $^7F_1$ (~593 nm), $^7F_2$ (~620 nm), $^7F_3$ (~650 nm) and $^7F_4$ (~700 nm) levels of Eu^{3+}. The TL spectra indicate that the trapped charge carriers - electrons and holes - recombine during the TL process at the Eu dopant [12,13]. The strong EPR signal at g = 2.023 is characteristic for a radical. Some weak, elusive EPR lines obtained at lower magnetic field [10] (not shown here) could not be unambiguously assigned to Eu^{2+} though its presence in the X-ray irradiated ceramics is expected as Eu^{3+} can act as electron trap.

The previous research suggested that holes generated upon ionizing radiation in the host lattice valence band are immobilized at O^{2-} ions (O_O^X) [14] giving rise to $O_o^\bullet$ traps of slightly different energies (distribution of trap depths) [15,16]. Trapping of an electron excited to the conduction band was then postulated to occur directly at the Eu^{3+} dopant, which would thus be converted into Eu^{2+} ion forming a Eu'_{Lu} defect site [10]. This is in agreement with the Dorenbos model [12,13,17–20] that predicts the ground state of Eu^{2+} in $LuPO_4$ to be positioned ~3.3 eV below the bottom of the host conduction band [13,21,22]. This makes the Eu^{3+} dopant a deep electron trap. The same model predicted that 5d excited state of Eu^{2+} is situated ~0.4 eV below conduction band. All these data are summarized in the energy level diagram presented in Fig. 2 [21,22].

However, convincing evidence that Eu^{2+} (Eu'_{Lu}) is generated upon

* Corresponding author.
E-mail address: eugeniusz.zych@chem.uni.wroc.pl (E. Zych).

https://doi.org/10.1016/j.jlumin.2018.11.050
Received 16 October 2018; Received in revised form 23 November 2018; Accepted 26 November 2018
Available online 27 November 2018

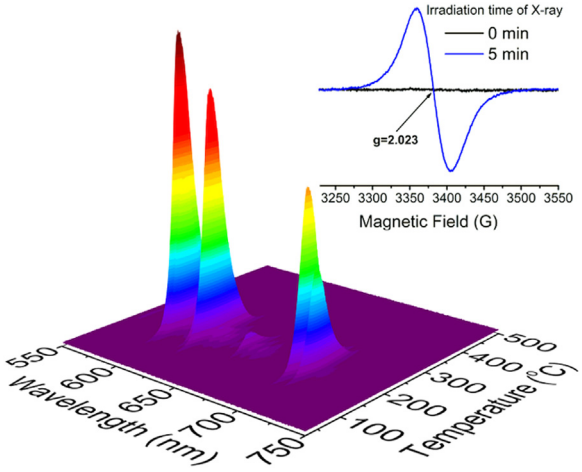

Fig. 1. The temperature- and wavelength-resolved TL of X-rayed $LuPO_4$:0.1% Eu ceramics. In the upper right corner EPR spectra before and after exposure of the material to X-rays is inserted [10].

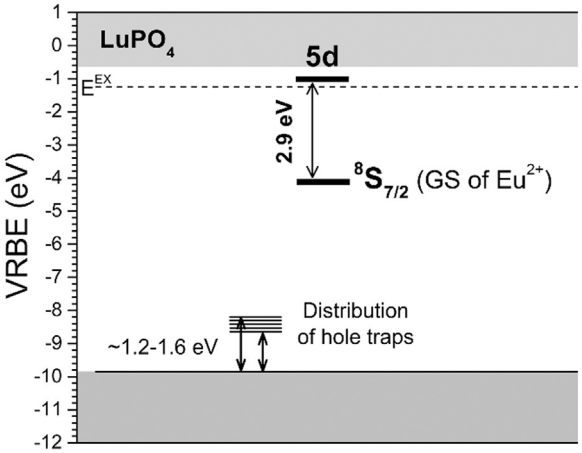

Fig. 2. Schematic depiction of the position of electronic levels of Eu^{2+} ground state together with estimated position of the $4f^65d^1$ excited state,[13] and the position of the distribution of hole trap depths estimated from previously published TL measurements [8,10].

X-ray irradiation of $LuPO_4$:Eu, was still missing. We considered photoluminescence (PL) spectroscopy a good tool to trace Eu^{2+} in the irradiated materials. However, as seen in Fig. 2 and given the ~0.5 eV uncertainty in the location of energy levels based on the Dorenbos model it was not clear if the $4f^65d^1$ excited state is indeed located below the $LuPO_4$ conduction band – a necessary condition for the 5d→4f luminescence of Eu^{2+} to be observed. On the other hand, Poolton et al. have already reported on low-temperature Sm^{2+} luminescence in doubly doped $LuPO_4$:Ce,Sm thermoluminescent material after its exposure to ionizing radiation [23]. This triggered our search for Eu^{2+} by luminescence spectroscopy.

Photoluminescence properties of Eu^{2+} are well known as they have been thoroughly investigated, also for practical applications. There is a vast number of materials in which the $4f^65d^1 \rightarrow 4f^7$ radiative relaxation of Eu^{2+} was reported both in photoluminescence and in scintillation [24–27]. The very important, widely applied storage phosphors, BaFBr:Eu and CsBr:Eu, are also activated with Eu^{2+} ions [28–37]. In addition many fluorescent lamp phosphors and white LED phosphors rely on $4f^65d$-$4f^7$ (d-f) emission from Eu^{2+}. However, emission from Eu^{2+} ions substituting a + 3 metal site in a host lattice is not very common [38,39].

The typical luminescence and excitation spectra of Eu^{2+} are composed of broad bands resulting from the interconfigurational $4f^65d^1 \leftrightarrow 4f^7$ transitions. The luminescence in oxides is usually located in the visible part of spectrum, mostly blue and green, occasionally yellow [24,40–42] and in composition with more covalent bonds (sulfide, nitrides) it tends to shift to red and even infrared [43–46]. A unique characteristic of Eu^{2+} spectroscopy was reported for MgF_2[24], CaF_2, SrF_2, and BaF_2 [47]. Namely, in low-temperature excitation spectra of these materials a set of narrow zero-phonon lines (ZPLs) related to transitions from the $^8S_{7/2}$ Eu^{2+} ground state to the ^7F_J Stark levels of the $4f^6(^7F_J)5d^1$ excited state were observed. The ZPLs were accompanied by vibronic components.

In this paper we investigate the Eu^{2+} generated in $LuPO_4$:Eu upon exposure to X-rays by photoluminescence measurements in the 20–300 K range. At low temperatures well-resolved fine structure in excitation and emission spectra is observed with sharp ZPLs and vibronic structure that reveals unprecedented detail in the electronic structure of the $4f^6(^7F_J)5d^1$ excited states of Eu^{2+} in $LuPO_4$. Room temperature (RT) infrared (IR) and electronic absorption spectra in UV–Vis region will also be exploited in analysis of these data and aid to assign specific lines to vibronic replicas.

2. Materials

The $LuPO_4$:x%Eu sintered materials (x = 0.1–2) were prepared using nanopowders precipitated from a water solution. In typical procedure the $Lu(NO_3)_3{\cdot}6H_2O$ and $Eu(NO_3)_3{\cdot}6H_2O$ were dissolved in water at 70–90 °C and then $(NH_4)_2HPO_4$ was added to precipitate the $LuPO_4$:Eu powders. The detailed procedure is described in [10]. Dried powders of $LuPO_4$:Eu were cold-pressed and sintered for 5 h at 1700 °C in vacuum. A representative pellet, before and after exposure to X-rays, is presented in the inset of Fig. 3. The sintered samples were slightly translucent which allowed to measure their absorption spectra, as described below.

3. Methods

Powder X-ray diffraction (XRD) patterns of sintered materials were recorded using a D8 Advance diffractometer from Bruker with Ni-filtered Cu radiation in the range of 2Θ = 10–70° and with a step of 2Θ = 0.008°. Photoluminescence emission (PL) and excitation (PLE) spectra and luminescence decay traces (DEC), were recorded in the range of 20–300 K with an FLS 980-sm Fluorescence Spectrometer from Edinburgh Instruments Ltd. using 450 W continuous Xenon arc lamp (PL and PLE) and EPLED-360 360 nm picosecond pulsed light emitting

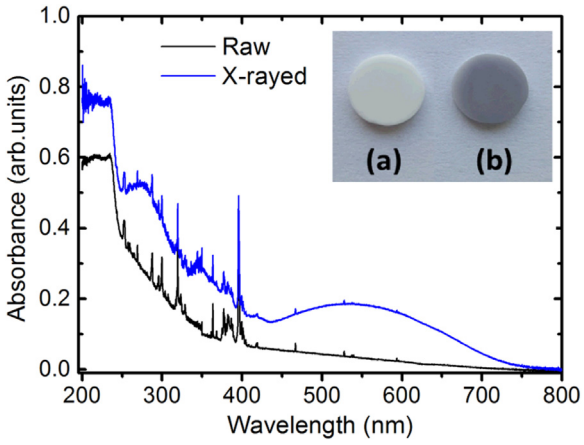

Fig. 3. Absorption spectra of a non-irradiated (black line) and an X-ray irradiated (blue line) $LuPO_4$:2%Eu pellet. Note, that scattering background at 800 nm was arbitrary subtracted for both spectra. The inset presents a picture of the non-irradiated (a), and irradiated (b) material (For interpretation of the references to color in this figure legend, the reader is referred to the web version of this article).

diode (DEC) as the excitation sources. TMS302-X Single Grating excitation and emission monochromators of 30 cm focal lengths were used and the luminescence light was recorded by Hamamatsu R928P high-gain photomultiplier (PM) detector. The luminescence decay traces were registered by means of F-G05PM featuring a Hamamatsu H5773-04 detector. Emission spectra were corrected for the spectral response of the emission detection system and excitation spectra were corrected for the variation in incident light intensity. The sample was mounted on a Lake Shore Cryotronics closed-cycle helium cryostat holder using Silver Adhesive 503 supplied by Electron Microscopy Sciences. Prior to measurements the specimens were irradiated at room temperature with white X-rays taken from a Cu X-ray tube working under the voltage of 40 kV and 5 mA current. The generated radiation was not filtered in any way. Absorption UV–Vis spectra were taken with a Cary 5000 SCAN UV–VIS–NIR spectrophotometer on a ~0.2 mm thick sample before and after exposure to X-rays from the same Cu tube. IR spectra were recorded with an IFS 66/s Bruker spectrometer in the range of 50–4000 cm^{-1} at room temperature (RT). Suspensions in nujol of spectral purity were used.

4. Results and discussion

The X-ray diffraction patterns of all obtained pellets with different Eu concentrations were presented in previous publications [8–10]. They are in excellent agreement with the data expected for tetragonal structure of $LuPO_4$ (ICSD #2025) [48].

4.1. Absorption spectra

Fig. 3 shows changes in UV–Vis absorption of the $LuPO_4$:2%Eu induced by irradiation with X-rays. For clarity, a background signal (samples were opaque) taken at 800 nm was subtracted from the respective spectra. The absorption spectrum of freshly sintered (not irradiated) material shows a number of sharp absorption lines in the visible and UV part of the spectrum that are assigned to the typical lines resulting from $4f^6 \rightarrow 4f^6$ parity-forbidden transitions of Eu^{3+} in $LuPO_4$ host [9,49]. Below about ~240 nm a strong broad band arises and this is assigned to the $O^{2-} \rightarrow Eu^{3+}$ charge transfer (CT) transition. Since the sintered pellet was not transparent an underlying background resulting from increasing scattering towards shorter wavelengths is observed. The irradiation of the material with X-rays caused significant graying of the pellet (see inset in Fig. 3) which was reflected by a new, very broad absorption band in the 400–750 nm range covering the full visible part of spectrum. Also in the UV region additional X-ray induced absorption bands are noticeable. This is the region where in many compositions Eu^{2+} absorbs due to $4f^7 \rightarrow 4f^6 5d^1$ parity-allowed transitions. Also from Dorenbos model [13,21,22] absorption of Eu^{2+} in $LuPO_4$ is expected in UV. All the absorption bands induced by X-rays disappeared after a short heating of the pellets to about 300 °C, as in TL experiments, and the white color of the sample was then restored. Such behavior indicates that the UV–Vis absorption features generated by the ionizing radiation are directly connected with charge carrier trapping (formation of color centers) in $LuPO_4$:Eu and its subsequent thermoluminescence releases the trapped charge carriers and the new bands vanish.

4.2. Photoluminescence spectroscopy

The energy level diagram in Fig. 2 shows that the $^8S_{7/2}$ ground state of Eu^{2+} in $LuPO_4$ is expected to be located 3.3 eV below the host conduction band [13]. Room temperature PL measurements on the X-ray irradiated $LuPO_4$:Eu pellet revealed the presence of a blue emission with two overlapping components peaking around 430 nm and 460 nm, see Fig. 4a. Neither of them was observed before exposure to X-rays. As observed in Fig. 4b, the intensity of both these PL bands systematically increased with the irradiation time with X-rays (ionizing radiation dose). The *relative* intensity of the broader band around 460 nm increased with the X-rays dose and reached the same peak height after 30 min of X-ray irradiation. Even higher doses hardly affected the intensities of both emissions, which indicates saturation.

The RT excitation spectrum of the 430 nm emission (Fig. 4a) was composed of two bands in UV part of spectrum and coinciding with the UV absorption induced by X-rays presented in Fig. 3. The longer-wavelength excitation band was clearly structured (black line in Fig. 4a). The PLE spectrum of the long-wavelength luminescence band (~460 nm) appeared in the same range of wavelengths but neither of its two components showed additional structure (red line in Fig. 4a). It is clear that both luminescent centers were generated upon the impact of the ionizing radiation.

Measurements at cryogenic temperatures were performed to provide more insight. Upon cooling clear changes are observed in the emission spectra (Fig. 4c). The 430 nm starts to show structure and the relative intensity increases. At 20 K the emission spectrum shows a sharp line at 425.8 nm and various lines at longer wavelengths. The sharp line at 425.8 nm is assigned to a zero-phonon transition from the lowest energy $4f^6(^7F_0)5d^1$ state to the $^8S_{7/2}$ ground state, in good agreement with the position predicted by Dorenbos [13]. The weaker lines at longer wavelengths are assigned to vibronic transitions. The low relative intensity in comparison to the ZPL indicates that the vibronic coupling is weak (small Huang-Rhys parameter, S) for the 4f-5d transition of Eu^{2+} in $LuPO_4$. Note that also for trivalent lanthanides in $LuPO_4$ (and YPO_4) the small relaxation in the $4f^{n-1}5d^1$ excited state allows for the observation of ZPLs and vibronic structure. At 20 K the 460 nm luminescence was no longer observed as a separate band. This is an interesting observation and requires further research that is out of the scope of this paper. We do not exclude that it is the so-called anomalous Eu^{2+} luminescence resulting from an impurity (Eu)-trapped exciton state. This hypothesis is supported by the fact that the $4f^6 5d^1$ excited level is positioned very close to conduction band. At elevated temperatures, this state may be thermally populated and give rise to trapped exciton emission Table 1.

To support the assignment of the vibronic emission lines observed in the PL spectrum at 20 K it is shown combined with the infrared spectrum in Fig. 4d. Most of the vibronic lines correspond with the host lattice vibrations. The strongest coupling was seen to the Lu-O modes (50–800 cm^{-1}), while coupling to the PO_4^{3-} vibrations were observed in the range of 800–1200 cm^{-1} [50]. A weaker coupling with PO_4^{3-} group vibrations is expected given the larger distance in comparison to vibrations involving interaction with the neighboring O^{2-} ions.

The Huang-Rhys parameter, S, characterizes the electron-phonon coupling for an electronic transition may be derived using the intensity of the ZPL, I_{ZPL}, and the total emission intensity I_0, according to Eq. (1). [51]

$$I_{ZPL} = I_0 \cdot \exp(-S). \quad (1)$$

From the low-temperature emission spectrum $S = 1.42$ was found, which indicates a weak electron-phonon coupling [24,51]. Based on the Huang-Rhys parameter S and the dominant vibrational mode (~315 cm^{-1}, see Fig. 4d) in the low-temperature emission spectrum the Stokes shift $SS = 2S \times 315\ cm^{-1} = \sim 900\ cm^{-1}$ was calculated [52]. Given the small Stokes shift and the variation in coupling strength for different vibrational modes it is not possible to give an accurate number for the Stokes shift. Theoretical calculations that are presently conducted explain 4f-5d spectra of Eu^{2+} and other lanthanide ions should aim to understand the details of the vibronic spectrum. At this point we conclude that the PL ~430 nm shows characteristics connected with Eu^{2+} luminescence with weak electron-phonon coupling and a remarkably small Stokes shift [53].

Strong changes were also observed in excitation spectra of the ~430 nm luminescence upon cooling the sample to 20 K, see Fig. 5a,b (compared to Fig. 4a). In the range of ~340–430 nm (Fig. 5a), a fine structure with sharp lines and many slightly broader features was

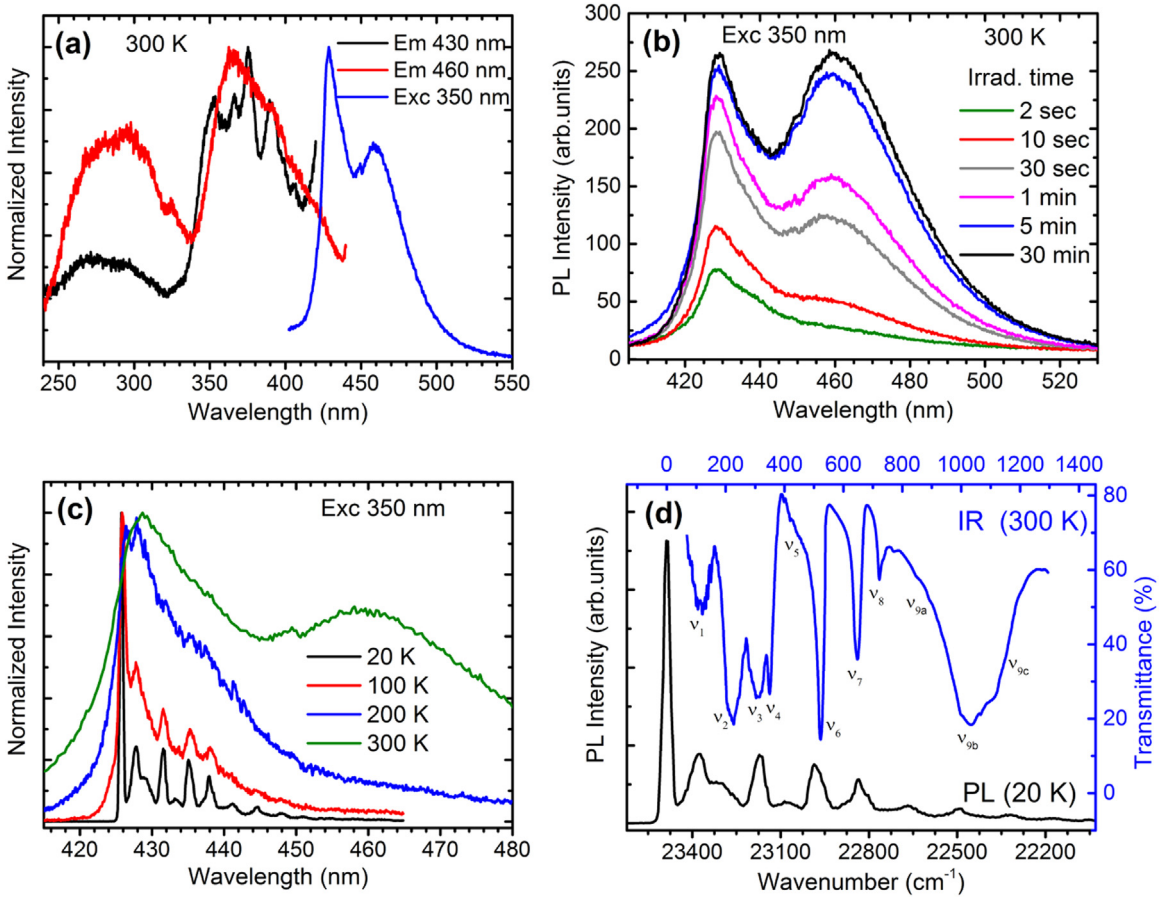

Fig. 4. Room temperature photoluminescence and excitation spectra of an X-ray irradiated $LuPO_4$:0.1% Eu pellet (a), dependence of the emission on the X-rays dose (irradiation time) (b), emission spectra upon 350 nm excitation at different temperatures (c) and 20 K PL spectrum upon 350 nm excitation combined with RT IR spectrum for vibronic progression analysis (d). See also Table 1.

Table 1
Positions of the zero-phonon and vibronic lines observed in the 20 K emission spectrum of the Eu^{2+} in X-ray irradiated $LuPO_4$:Eu. The vibronic lines are labeled 1, 2, 3, 4, 5, 6, 7, 8, 9 according to increasing energy of the vibration.

Transition	Emission spectral position		Energy difference with respect to ZPL (cm^{-1})
	λ (nm)	E (cm^{-1})	
$4f^6(^7F_0)5d^1 \rightarrow {}^8S_{7/2}$	425.80	23,486.55	0
ν_1	427.90	23,370.90	115.60
ν_2	429.70	23,272.80	213.70
ν_3	431.55	23,171.90	314.65
ν_5	433.60	23,061.70	424.85
ν_6	435.30	22,971.50	515.05
ν_7	437.80	22,840.30	646.25
ν_{9a}	441.35	22,656.75	829.80
ν_{9b}	444.80	22,480.75	1005.80
ν_{9c}	447.90	22,325.10	1161.45

observed. Taking into account the FWHM of the observed lines and their relative intensities they might be divided into two categories: (i) very narrow, mostly strong lines (probably ZPLs) and (ii) noticeably broader and less intense components at specific energies from ZPLs (identified as vibronic lines). The overall fine structure covered a region of about 6500 cm^{-1} (see Fig. 5b), which is close to the energy spanned by the levels of the $^7F_{0-6}$ multiplet of Eu^{3+} [54,55].

The fine structure in the low-temperature PLE spectrum reflects transitions to the $4f^6(^7F_J)$ electronic origins of the $4f^65d^1$ excited configuration of Eu^{2+}, as previously reported for some fluorides, though those spectra were less resolved and showed a much smaller number of $4f^6(^7F_J)5d^1$ lines [24,47]. In Fig. 5a the lines identified as ZPLs are indicated with letters (starting with a) for each of the ^7F_J multiplets. It is interesting to compare the splitting of the $4f^6$ core in the $4f^65d^1$ excited state with that of the $4f^6$ core of Eu^{3+} in $LuPO_4$. The two spectra drawn on an energy scales are presented in Fig. 5b. The overall correspondence of both spectra is evident but upon a detailed comparison it becomes clear that the ^7F_J splitting is different for the $4f^6$ configuration in the $4f^65d^1$ state of Eu^{2+} compared to that for the $4f^6$ configuration of Eu^{3+}. In the case of the $^8S_{7/2} \rightarrow 4f^6(^7F_J)5d^1$ transitions the splitting of the components of different J is slightly larger (see Fig. 5b), which is due to an influence of the 5d-configuration on f-electrons in the Eu^{2+} $4f^65d^1$ excited state. The shielding by and interaction with the 5d electronic wavefunctions also causes a different crystal field splitting within the ^7F_J terms.

The present observations present an ideal model system for testing energy level calculations for the $4f^65d^1$ states of Eu^{2+}. Presently a variety of theoretical approaches is developed to calculate the energy level structure and relaxation in $4f^{n-1}5d^1$ states of lanthanide ions. The clear observation of ZPLs for individual $4f^6(^7F_J)5d$ levels make $LuPO_4$:Eu^{2+} an excellent system to validate the various theoretical approaches that will be more conclusive than comparison with structureless broad bands that are usually observed in Eu^{2+} excitation spectra. In the literature there are a few examples where similar observations were reported in other compositions (mostly fluorides), though the previously published spectra with $4f^6(^7F_J)5d^1$ ZPLs only included a small number of lines for the lower ^7F_J multiplets [24,47].

A detailed overview of the assignment of the sharp lines observed in the excitation spectrum in Fig. 5 is provided in the Supporting Info (Table S1). To assign lines to ZPLs we selected excitation lines that are

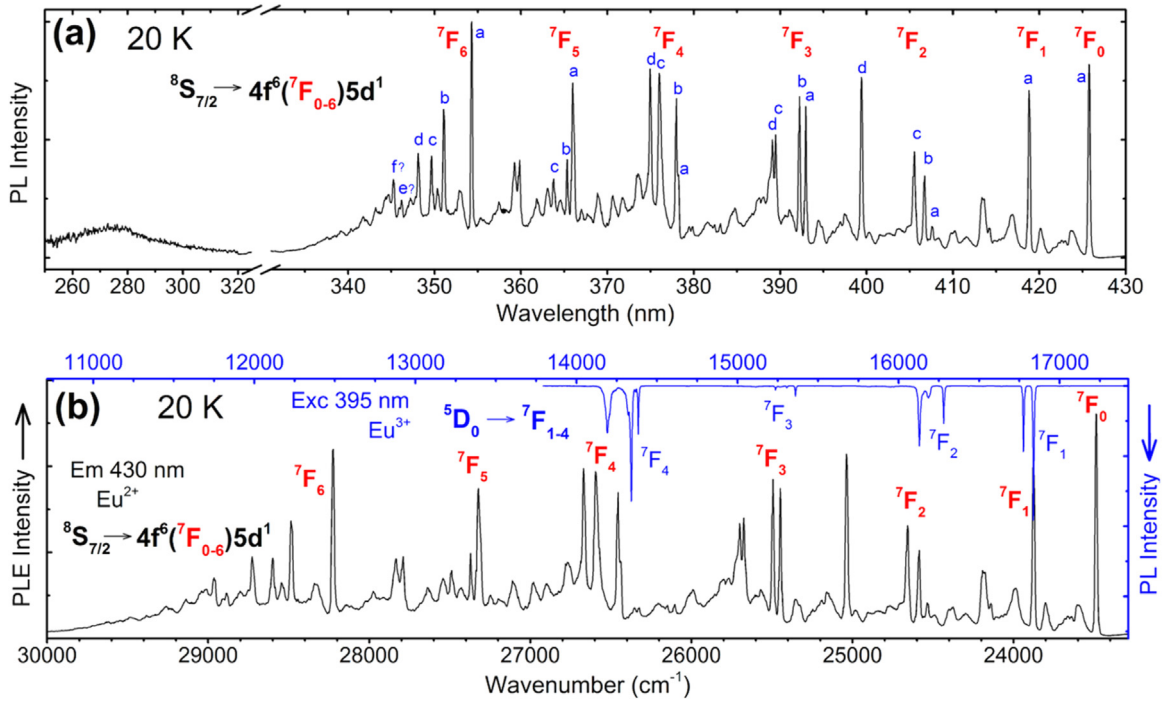

Fig. 5. The 20 K temperature PLE spectrum of Eu^{2+} emission of $LuPO_4$:0.1%Eu material irradiated with X-rays (a), and the same spectrum drawn on an energy scale with overlayed 20 K PL emission of Eu^{3+} in the same material under 395 nm excitation (blue line) (b). The a,b,c,d,e,f in (a) depict lines that are assigned to zero-phonon excitation lines related to the Stark level of the $^7F_{0-6}$ electronic configuration of the $4f^6(^7F_{0-6})5d^1$ excited state. Positions e and f ZPLs are dubious. The assignment is based on the sharpness of the lines and the observation of vibronic lines at specific distances from these ZPLs.

clearly narrower than others. They are labeled with letters a-f for each ^7F_J multiplet of the $4f^6(^7F_J)5d^1$ excited state of Eu^{2+} in Fig. 5a. In addition we associated many of the vibronic transitions to the electronic origins. In Fig. 6a,b,c examples of this analysis based on the energy vibrations found in the infrared spectrum are presented for the $^8S_{7/2} \rightarrow 4f^6(^7F_0)5d^1$, $^8S_{7/2} \rightarrow 4f^6(^7F_1)5d^1$ and $^8S_{7/2} \rightarrow 4f^6(^7F_2)5d^1$ transitions. Analogous procedures were used for the $^8S_{7/2} \rightarrow 4f^6(^7F_{3-6})5d^1$ transitions and these are presented in the Supporting information in Figs. S1-S4.

With increasing J-number vibronic transitions connected with different Stark levels of various ^7F_J states overlap and mix. Consequently, an unambiguous assignment of the vibronic lines becomes difficult. Therefore, in Table S1 where we summarize the results of the analysis described above some of the assignments are still ambiguous. The resulting energies for the ZPLs of $4f^6(^7F_J)5d$ states and vibronic replicas given in Table S1 can serve as input and reference data for detailed theoretical calculations of the $4f^65d^1$ energy level calculations.

4.3. Temperature dependence of the Eu^{2+} PL kinetics

The temperature dependent emission spectra revealed a clear increase of the 430 nm Eu^{2+} emission band upon cooling from RT to 20 K. This indicates that the emission is partly quenched at RT. To gain insight in the quenching behavior, luminescence decay measurements are a powerful tool.[52] In Fig. 7a the Eu^{2+} emission decay curves of the X-rayed $LuPO_4$:0.1%Eu sintered material in the 20–300 K temperature range are presented for pulsed ps excitation at 360 nm.

Between 20 K and ~175 K the decays are very similar, nearly single exponential. At higher temperatures a shortening of emission decays is observed and fitting required a two-exponential function to reproduce the faster initial decay. The shortening of the life time can be explained by thermal quenching in the range of ~175–300 K. Dependence of the derived decay times (averaged, where needed) on temperature is presented in Fig. 7b. The experimental points could be fitted (black line in Fig. 7b) by Eq. (2) [56,57]:

$$p = \frac{1}{\tau} = \frac{1}{\tau_r} + \frac{1}{\tau_{nr}} \exp\left(-\Delta E_a / kT\right) \quad (2)$$

where p is the transition rate, τ is its decay time at temperature T, $1/\tau_r$ is the probability of radiative transition in the absence of thermal quenching, $1/\tau_{nr}$ is the probability of non-radiative decay, k is the Boltzmann constant, and ΔE_a is the activation energy of thermal quenching. $\Delta E_a = 0.25 \pm 0.01$ eV was found from the fit.

The radiative decay time below 175 K is τ ~220–230 ns, which is rather short for Eu^{2+} $4f^65d^1$ luminescence. Typically the Eu^{2+} emission radiative decay varies between 700 ns and 2000 ns with longer life times for longer emission wavelengths [58,59]. Shorter radiative life times have also been reported, e.g. in the case of X-rayed YAG:Eu, the decay time of the Eu^{2+} emission was ~450 ns [38] and in a series of $ALnS_2$:Eu (A = Na, K, Rb and Ln=La, Gd, Lu, Y) sulfides it was within ~400–700 ns range [39]. It is not clear why the lifetime of the Eu^{2+} emission is almost a factor 2 shorter than expected in the present case. The temperature dependent lifetime measurements do show a clear quenching of the Eu^{2+} emission above 170 K. The mechanism for quenching is probably thermally activated photoionization. The position of the $4f^65d^1$ excited state of Eu^{2+} is estimated to be ~0.4 eV below the conduction band in $LuPO_4$. The activation energy for thermal quenching from the $4f^65d^1$ state of 0.25 eV is in excellent agreement with this value, also because the thermal energy barrier is always smaller than the barrier determined from optical data in which relaxation effects that lower the barrier are not taken into account. The mechanism for quenching is thermal release of the electron from the $4f^65d^1$ excited state after photoexcitation.

5. Conclusions

$LuPO_4$:Eu sintered at high temperatures is an efficient storage phosphor with a single thermoluminescence band peaking around 200 °C. Electrons are trapped at Eu^{3+} site converting it to Eu^{2+}. Holes are immobilized around O^{2-} ions. Heating the material to ~200 °C

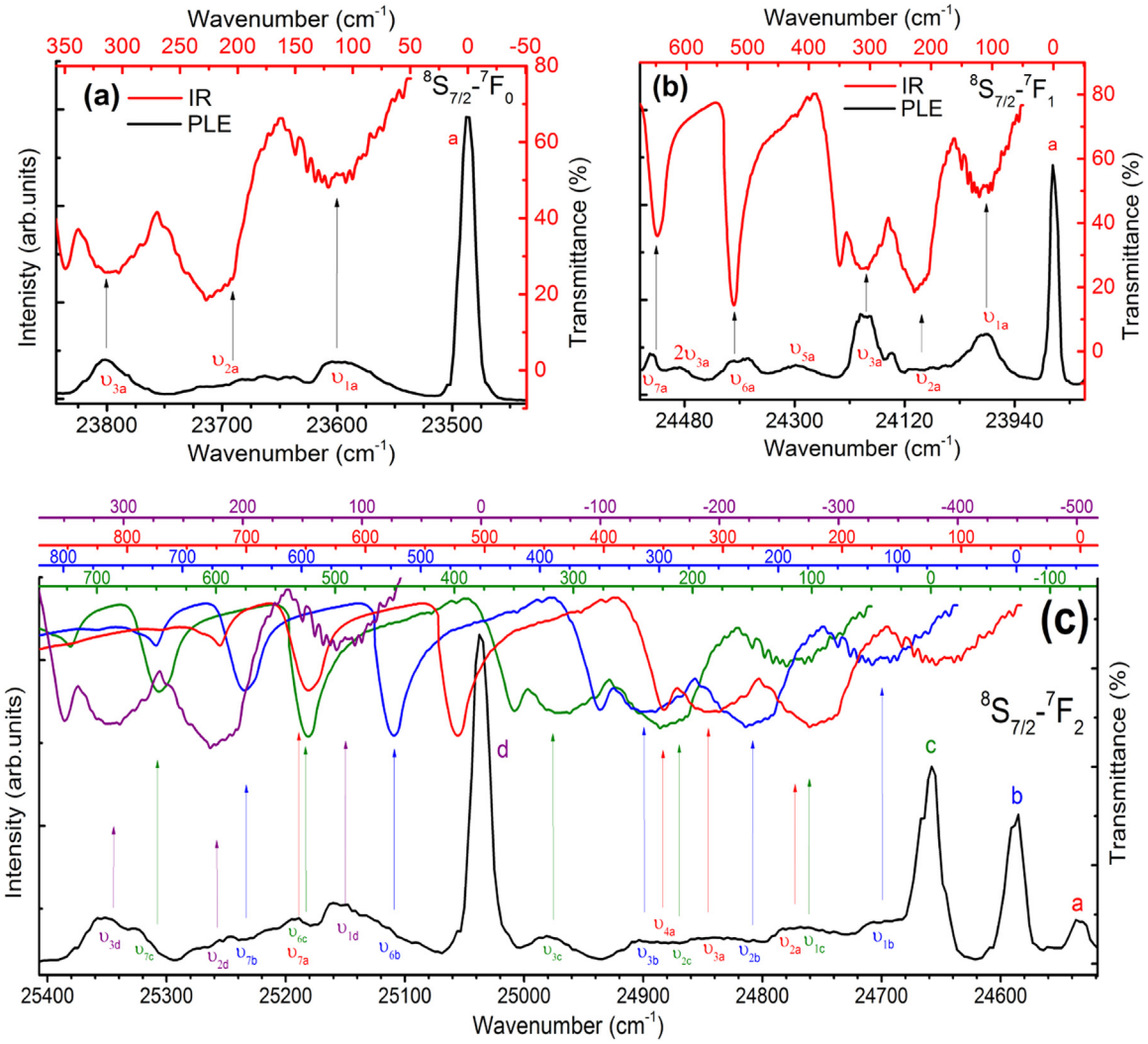

Fig. 6. The 20 K excitation spectra of $LuPO_4$:0.1% Eu irradiated with X-rays for the $^8S_{7/2}\rightarrow{}^7F_0$ (a), $^8S_{7/2}\rightarrow{}^7F_1$ (b), and $^8S_{7/2}\rightarrow{}^7F_2$ (c) transitions together with RT IR spectrum (color lines). The a, b, c, d letters in the c) spectra indicate four crystal field components (zero-phonon transitions) within the $^8S_{7/2}\rightarrow{}^7F_2$ range. Position of vibronic lines in the excitation spectra are also indicated as $\nu_{\#}$ (see Table 1 for details).

releases trapped holes and recombination at Eu-sites results in orange-red luminescence from Eu^{3+} ions.

New evidence for the formation of Eu^{2+} is obtained from optical measurements. The X-ray irradiated sample showed a set of new broad-band absorptions covering the visible and UV part of the spectrum. Under UV excitation of $LuPO_4$:Eu blue band emission is observed at 300 K. The excitation spectrum of the emission shows features characteristic of Eu^{2+}. Upon cooling, fine structure appears in the emission spectrum with a sharp and intense zero-phonon line peaking at 425.8 nm and vibronic lines at lower energies, coinciding with

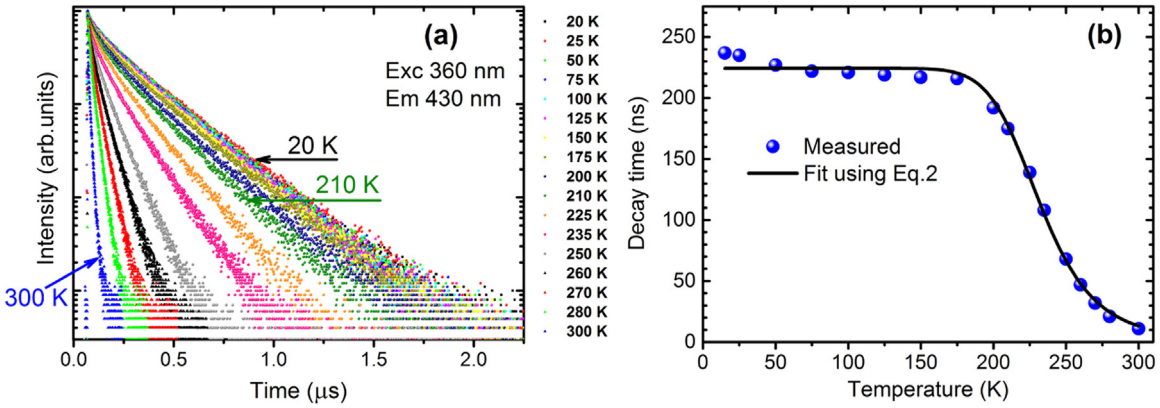

Fig. 7. The decay traces of 430 nm emission under 360 nm excitation of X-rayed $LuPO_4$:0.1%Eu material in the temperature range of 20–300 K (a). The temperature dependence of the decay times with Arrhenius-type fit (black line) (b).

vibrational energies observed in the IR-spectrum of the $LuPO_4$ host. The 20 K excitation spectrum of the Eu^{2+} luminescence in X-ray irradiated $LuPO_4$:Eu reveals remarkably rich fine structure with many sharp lines. The spectrum was analyzed by assigning the narrow excitation lines to transitions to $4f^6(^7F_J)5d^1$ states. Spin-orbit and crystal field splitting of the $4f^6(^7F_J)$ core explains the large number of zero-phonon lines. On the higher energy side of the electronic origins slightly broader spectral features could be assigned to vibronic side bands.

The analysis shows that the splitting of the ^7F_J levels in the $4f^65d^1$ excited state is different from the splitting of the ^7F_J levels of the $4f^6$ core of Eu^{3+}. This observation provides direct evidence for the role of $4f^6$-5d interaction on the ^7F_J splitting. With the present analysis the energy level structure of the full $4f^6(^7F_J)5d^1$ excited state of Eu^{2+} is resolved in detail and can serve as input for comparison with results from theoretical calculations of $4f^{n-1}5d^1$ states of lanthanide ions to test the various models that are presently applied and developed.

Acknowledgments

This work was supported by the Polish National Science Centre (NCN) under the grant # UMO-2015/19/N/ST5/00784 which is gratefully acknowledged.

Supplemental material description

The Supporting information file contains four figures presenting excitation spectra of Eu^{2+} luminescence in the region of $^8S_{7/2}\rightarrow 4f^6(^7F_3)5d^1$ (Fig. S1), $^8S_{7/2}\rightarrow 4f^6(^7F_4)5d^1$ (Fig. S2), $^8S_{7/2}\rightarrow 4f^6(^7F_5)5d^1$ (Fig. S3), $^8S_{7/2}\rightarrow 4f^6(^7F_6)5d^1$ (Fig. S4) in $LuPO_4$:Eu irradiated with X-rays taken at 20 K. IR spectra are enclosed to show the host vibrations and their use in analysis of vibronic progression in the excitation spectrum. Table S1 lists positions of identified zero-phonon and vibronic lines.

Appendix A. Supporting information

Supplementary data associated with this article can be found in the online version at https://doi.org/10.1016/j.jlumin.2018.11.050.

References

[1] G.M. Williams, P.C. Becker, J.G. Conway, N. Edelstein, L.A. Boatner, M.M. Abraham, Intensities of electronic Raman scattering between crystal-field levels of Ce^{3+} in $LuPO_4$: nonresonant and near-resonant excitation, Phys. Rev. B 40 (2008) 4132–4142.
[2] A. Lempicki, A.J. Wojtowicz, C. Brecher, Inorganic scintillators, in: S.R. Rotman (Ed.), Wide-Gap Lumin. Mater. Theory Appl, 1997, pp. 237–301.
[3] A.J. Wojtowicz, A. Lempicki, D. Wisniewski, L.A. Boatner, Cerium-doped orthophosphate scintillators, Mat. Res. Soc. Symp. Proc. 348 (1994) 123–129.
[4] A. Rapaport, V. David, M. Bass, C. Deka, L.A. Boatner, Optical spectroscopy of erbium-doped lutetium orthophosphate, J. Lumin. 85 (1999) 155–161, https://doi.org/10.1016/S0022-2313(99)00060-5.
[5] J. Cybińska, M. Woźniak, A. Mudring, E. Zych, Controllable synthesis of nanoscale YPO_4:Eu^{3+} in ionic liquid, J. Lumin. 169 (2016) 868–873.
[6] K. Srinivasu, R.S. Ningthoujam, V. Sudarsan, R.K. Vatsa, A.K. Tyagi, P. Srinivasu, A. Vinu, Eu^{3+} and Dy^{3+} doped YPO_4 nanoparticles: low temperature synthesis and luminescence studies, J. Nanosci. Nanotechnol. 9 (2009) 3034–3039, https://doi.org/10.1166/jnn.2009.026.
[7] S.V. Ushakov, K.B. Helean, A. Navrotsky, L.A. Boatner, Thermochemistry of rare-earth orthophosphates, J. Mater. Res. 16 (2001) 2623–2633.
[8] E. Zych, D. Kulesza, J. Zeler, J. Cybińska, K. Fiaczyk, A. Wiatrowska, SrS:Ce and $LuPO_4$:Eu Sintered Ceramics: old Phosphors with New Functionalities, ECS J. Solid State Sci. Technol. 5 (2015) R3078–R3088, https://doi.org/10.1149/2.0101601jss.
[9] J. Zeler, J. Cybińska, E. Zych, A new photoluminescent feature in $LuPO_4$:Eu thermoluminescent sintered materials, RSC Adv. 6 (2016) 57920–57928, https://doi.org/10.1039/C6RA09588G.
[10] J. Zeler, E. Zych, On the thermoluminescence properties and mechanism of $LuPO_4$:Eu sintered materials, RSC Adv. 6 (2016) 89019–89027, https://doi.org/10.1039/C6RA18804D.
[11] V.S. Levushkina, D.A. Spassky, E.M. Aleksanyan, M.G. Brik, M.S. Tretyakova, B.I. Zadneprovski, A.N. Belsky, Bandgap engineering of the $Lu_xY_{1-x}PO_4$ mixed crystals, J. Lumin. 171 (2016) 33–39, https://doi.org/10.1016/j.jlumin.2015.10.074.
[12] A.J.J. Bos, P. Dorenbos, A. Bessière, B. Viana, Lanthanide energy levels in YPO_4, Radiat. Meas. 43 (2008) 222–226, https://doi.org/10.1016/j.radmeas.2007.10.042.
[13] A.H. Krumpel, A.J.J. Bos, A. Bessière, E. Van der Kolk, P. Dorenbos, Controlled electron and hole trapping in YPO_4:Ce^{3+},Ln^{3+} and $LuPO_4$:Ce^{3+},Ln^{3+} (Ln=Sm, Dy, Ho, Er, Tm), Phys. Rev. B 80 (2009) 085103, https://doi.org/10.1103/PhysRevB.80.085103.
[14] N.G. Connelly, R.M. Hartshorn, T. Damhus, A.T. Hutton, Nomenclature of Inorganic Chemistry, Royal Society of Chemistry, UK, 2005 (Published for the International Union of Pure and Applied Chemistry by The Royal Society of Chemistry, Printed by Biddles Ltd, King's Lynn, Norfolk, UK. ISBN 0-85404-438-8).
[15] S.W.S. McKeever, Thermoluminescence of Solids, Cambridge University Press, Cambridge, U.K, 1985.
[16] R. Chen, S.W.S. McKeever, Theory of Thermoluminescence and Related Phenomena, World Scientific Publishing Co. Pte. Ltd., Singapore, 1997.
[17] T. Shalapska, P. Dorenbos, A. Gektin, G. Stryganyuk, A. Voloshinovskii, Luminescence spectroscopy and energy level location of lanthanide ions doped in La$(PO_3)_3$, J. Lumin. 155 (2014) 95–100, https://doi.org/10.1016/j.jlumin.2014.06.029.
[18] P. Dorenbos, The electronic level structure of lanthanide impurities in $REPO_4$, $REBO_3$, $REAlO_3$, and RE_2O_3 (RE = La, Gd, Y, Lu, Sc) compounds (225501-1-225501–225507), J. Phys. Condens. Matter 25 (2013), https://doi.org/10.1088/0953-8984/25/22/225501.
[19] A.H. Krumpel, E. Van der Kolk, E. Cavalli, P. Boutinaud, M. Bettinelli, P. Dorenbos, Lanthanide 4f-level location in AVO_4): ln($^{3+}$) (A = La, Gd, Lu) crystals (115503-1-115503–115508), J. Phys. Condens. Matter 21 (2009), https://doi.org/10.1088/0953-8984/21/11/115503.
[20] P. Dorenbos, A.J.J. Bos, N.R.J. Poolton, Electron transfer processes in double lanthanide activated YPO_4, Opt. Mater. 33 (2011) 1019–1023, https://doi.org/10.1016/j.optmat.2010.08.016.
[21] P. Dorenbos, Modeling the chemical shift of lanthanide 4f electron binding energies, Phys. Rev. B Condens. Matter Mater. Phys. 85 (2012) 1–10, https://doi.org/10.1103/PhysRevB.85.165107.
[22] P. Dorenbos, Charge transfer bands in optical materials and related defect level location, Opt. Mater. 69 (2017) 8–22, https://doi.org/10.1016/j.optmat.2017.03.061.
[23] N.R.J. Poolton, A.J.J. Bos, P. Dorenbos, Luminescence emission from metastable Sm^{2+} defects in YPO_4:Ce,Sm, J. Phys. Condens. Matter 24 (2012) 225502, https://doi.org/10.1088/0953-8984/24/22/225502.
[24] S. Lizzo, A.H. Velders, A. Meijerink, G.J. Dirksen, G. Blasse, The luminescence of Eu^{2+} in magnesium fluoride crystals, J. Lumin. 65 (1995) 303–311, https://doi.org/10.1016/0022-2313(95)00080-1.
[25] P. Leblans, L. Struye, S. Elen, I. Mans, H. Vrielinck, F. Callens, X-ray enhancement of CsI:Eu^{2+} radioluminescence, J. Lumin. 165 (2015) 68–76, https://doi.org/10.1016/j.jlumin.2015.04.016.
[26] J. Rubio O, Doubly-valent rare-earth ions in halide crystals, J. Phys. Chem. Solids 52 (1991) 101–174, https://doi.org/10.1016/0022-3697(91)90062-5.
[27] H. Winkler, Q. Trinh Vinh, T. Quoc Khanh, A. Benker, C. Bois, R. Petry, A. Zych, LED components - principles of radiation generation and packing, in: T.Q. Khanh, P. Bodrogi, Q.T. Vinh, H. Winkler (Eds.), LED Light, Wiley-VCH, 2015(ISBN: 978-3-527-41212-9. Printing and Binding Markono Print Media Pte Ltd, Singapore).
[28] P. Jakes, J. Zimmermann, H. Von Seggern, A. Ozarowski, J. Van Tol, R.-A. Eichel, Eu^{2+} -doped CsBr photostimulable X-ray storage phosphors - analysis of defect structure by high-frequency EPR (1350073-1-1350073–1350074), Funct. Mater. Lett. 7 (2014), https://doi.org/10.1142/S1793604713500732.
[29] M. Batentschuk, A. Winnacker, K. Schwartz, C. Trautmann, Storage efficiency of BaFBr:Eu^{2+} image plates irradiated by swift heavy ions, J. Lumin. 125 (2007) 40–44, https://doi.org/10.1016/j.jlumin.2006.08.023.
[30] M. Koshimizu, H. Hori, K. Asai, Photostimulated luminescence properties of BaFBr:Eu under ion irradiation, Radiat. Meas. 71 (2014) 113–116, https://doi.org/10.1016/j.radmeas.2014.03.005.
[31] A.A. Shalaev, E.A. Radzhabov, Single crystal growth of BaFBr:Eu storage phosphor with alkali impurities, J. Cryst. Growth 275 (2005) 2004–2006, https://doi.org/10.1016/j.jcrysgro.2004.11.092.
[32] M. Salis, On the photo-stimulated luminescence of BaFBr:Eu^{2+} phosphors, J. Lumin. 104 (2003) 17–25, https://doi.org/10.1016/S0022-2313(02)00660-9.
[33] J.-M. Spaeth, Recent developments in X-ray storage phosphor materials, Radiat. Meas. 33 (2001) 527–532, https://doi.org/10.1016/S1350-4487(01)00050-6.
[34] M. Xianguo, W. Yongsheng, J. Hui, S. Li, A new promising X-ray storage phosphor BaBrCl:Eu^{2+}, J. Rare Earths 24 (2006) 503–505.
[35] S. Schweizer, M. Secu, J.M. Spaeth, L.W. Hobbs, A. Edgar, G.V.M. Williams, New developments in X-ray storage phosphors, Radiat. Meas. 38 (2004) 633–638, https://doi.org/10.1016/j.radmeas.2003.12.025.
[36] M.Z. Su, W. Zhao, W. Chen, Y. Dong, J.H. Lin, X-ray storage phosphors, their properties and mechanism, J. Alloy. Compd. 225 (1995) 539–543, https://doi.org/10.1016/0925-8388(94)07059-8.
[37] A. Meijerink, Photostimulated luminescence and thermally stimulated luminescence of (Ba,Sr)$F_{1+x}Rr_{1-x}$-Eu^{2+}, Mater. Chem. Phys. 44 (1996) 170–177, https://doi.org/10.1016/0254-0584(95)01672-H.
[38] L. Havlák, J. Bárta, M. Buryi, V. Jarý, E. Mihóková, V. Laguta, P. Boháček, M. Nikl, Eu^{2+} Stabilization in YAG structure: optical and electron paramagnetic resonance study, J. Phys. Chem. C 120 (2016) 21751–21761, https://doi.org/10.1021/acs.jpcc.6b06397.
[39] V. Jarỳ, L. Havlák, J. Bárta, M. Buryi, E. Mihóková, M. Rejman, V. Laguta, M. Nikl, Optical, structural and paramagnetic properties of Eu-doped ternary sulfides $ALnS_2$ (A = Na, K, Rb; Ln = La, Gd, Lu, Y), Materials 8 (2015), pp. 6978–6998, https://doi.org/10.3390/ma8105348.

[40] H. Guo, W. Chen, W. Zeng, Y. Wang, Y. Li, A long-lasting phosphor $Ba_3P_4O_{13}$: Eu^{2+}, ECS Solid State Lett. 4 (2014) R1–R3, https://doi.org/10.1149/2.0051501ssl.
[41] V. Singh, J.J. Zhu, M. Tiwari, M. Soni, M. Aynayas, S.H. Hyun, R. Narayanan, M. Mohapatra, V. Natarajan, Characterization, luminescence and EPR investigations of Eu^{2+} activated strontium aluminate phosphor, J. Non Cryst. Solids 355 (2009) 2491–2495, https://doi.org/10.1016/j.jnoncrysol.2009.08.027.
[42] A. Madej, E. Zych, Controlled synthesis of the monoclinic and orthorhombic polymorphs of Sr_2SiO_4 activated with Ce^{3+} or Eu^{2+}, RSC Adv. 5 (2015) 104441–104450, https://doi.org/10.1039/C5RA21573K.
[43] P. Pust, V. Weiler, C. Hecht, A. Tücks, A.S. Wochnik, A.-K. Henß, D. Wiechert, C. Scheu, P.J. Schmidt, W. Schnick, Narrow-band red-emitting $Sr[LiAl_3N_4]:Eu^{2+}$ as a next-generation LED-phosphor material, Nat. Mater. 13 (2014) 891–896, https://doi.org/10.1038/nmat4012.
[44] P. Strobel, V. Weiler, C. Hecht, P.J. Schmidt, W. Schnick, Luminescence of the Narrow-band Red Emitting Nitridomagnesosilicate $Li_2(Ca_{1-x}Sr_x)_2[Mg_2Si_2N_6]:Eu^{2+}$ (x = 0–0.06) (acs.chemmater.6b05196), Chem. Mater. 2 (2017), https://doi.org/10.1021/acs.chemmater.6b05196.
[45] P. Strobel, S. Schmiechen, M. Siegert, A. Tücks, P.J. Schmidt, W. Schnick, Narrow-band green emitting nitridolithoalumosilicate $Ba[Li_2(Al_2Si_2)N_6]:Eu^{2+}$ with framework topology whj for LED/LCD-backlighting applications, Chem. Mater. 27 (2015) 6109–6115, https://doi.org/10.1021/acs.chemmater.5b02702.
[46] A. Marchuk, S. Wendl, N. Imamovic, F. Tambornino, D. Wiechert, P.J. Schmidt, W. Schnick, Nontypical luminescence properties and structural relation of $Ba_3P_5N_{10}X:Eu^{2+}$ (X = Cl, I): nitridophosphate halides with zeolite-like structure, Chem. Mater. 27 (2015) 6432–6441, https://doi.org/10.1021/acs.chemmater.5b02668.
[47] L.L. Chase, Microwave-optical double resonance of the metastable 4f65d level of Eu^{2+} in the fluorite lattices, Phys. Rev. B 2 (1970) 2308–2318, https://doi.org/10.1103/PhysRevB.2.2308.
[48] Inorganic Crystal Structure Database (ICSD#2025), Fachinformationszentrum Karlsruhe, Germany, 2015.
[49] I.E. Seferis, J. Zeler, C. Michail, I. Valais, G. Fountos, N. Kalyvas, A. Bakas, I. Kandarakis, E. Zych, On the response of semitransparent nanoparticulated films of $LuPO_4$:Eu in poly-energetic X-ray imaging applications, Appl. Phys. A 122 (2016) 1–10.
[50] P. Savchyn, I. Karbovnyk, V. Vistovskyy, A. Voloshinovskii, V. Pankratov, M. Cestelli Guidi, S. Mirri, O. Myahkota, A. Riabtseva, N. Mitina, A. Zaichenko, A.I. Popov, Vibrational properties of $LaPO_4$ nanoparticles in mid- and far-infrared domain (124309-1-124309–6), J. Appl. Phys. 112 (2012), https://doi.org/10.1063/1.4769891.
[51] G. Blasse, Vibronic transitions in rare earth spectroscopy, Int. Rev. Phys. Chem. 11 (1992) 71–100, https://doi.org/10.1080/01442359209353266.
[52] V. Bachmann, C. Ronda, A. Meijerink, Temperature quenching of yellow Ce^{3+} luminescence in YAG:Ce, Chem. Mater. 21 (2009) 2077–2084, https://doi.org/10.1021/cm8030768.
[53] G. Blasse, B.C. Grabmaier, Luminescent Materials, Springer-Verlag Berlin Heidelberg, 1994,, https://doi.org/10.1021/cm00003a005 (ISBN 978-3-540-58019-5. Printed in Germany).
[54] G.H. Dieke, Spectra and energy levels of rare earth ions in crystals, Am. J. Phys. 38 (1963) 399, https://doi.org/10.1119/1.1976350.
[55] W.T. Carnall, G.L. Goodman, K. Rajnak, R.S. Rana, A systematic analysis of the spectra of the lanthanides doped into single crystal LaF_3, J. Chem. Phys. 90 (1989) 3443–3457, https://doi.org/10.1063/1.455853.
[56] M. Yamaga, Y. Ohsumi, T. Nakayama, T.P.J. Han, Persistent phosphorescence in Ce-doped Lu_2SiO_5, Opt. Mater. Express 2 (2012) 413–419, https://doi.org/10.1364/OME.2.000413.
[57] A.K. Prasad, M. Kook, M. Jain, Probing metastable Sm^{2+} and optically stimulated tunnelling emission in YPO_4:Sm,Ce, Radiat. Meas. 106 (2016) 61–66, https://doi.org/10.1016/j.radmeas.2016.11.012.
[58] S.H.M. Poort, A. Meyerink, G. Blasse, Lifetime measurements in Eu^{2+}-doped host lattices, J. Phys. Chem. Solids 58 (1997) 1451–1456, https://doi.org/10.1016/S0022-3697(97)00010-3.
[59] B. Henderson, G.F. Imbusch, Optical Spectroscopy of Inorganic Solids, Oxford science Publications, Clarendon Press, Oxford, 1989 (ISBN: 9780199298624. Printed in Great Britten, Biddles Ltd. King's Lynn, Norfolk).